4 Basic bluff-body aerodynamics

4.1 Flow around bluff bodies

Structures of interest in this book can generally be classified as *bluff* bodies with respect to the air flow around them, in contrast to *streamlined* bodies, such as aircraft wings and yacht sails (when the boat is sailing across the wind). Figure 4.1 shows the flow patterns around an airfoil (at low angle of attack), and around a two-dimensional body of rectangular cross-section. The flow patterns are shown for steady free-stream flow; turbulence in the approaching flow, which occurs in the atmospheric boundary-layer, as discussed in Chapter 3, can modify the flow around a bluff body, as will be discussed later.

It can be seen in Figure 4.1 that the flow streamlines around the airfoil follow closely the contours of the body. The free-stream flow is separated from the surface of the airfoil only by a thin boundary layer, in which the tangential flow is brought to rest at the surface. The flow around the rectangular section (a typical bluff body) in Figure 4.1 is characterized by a 'separation' of the flow at the leading edge corners. The separated flow region is divided from the outer flow by a thin region of high shear and vorticity, a region known as a free shear layer, which is similar to the boundary layer on the airfoil, but not attached

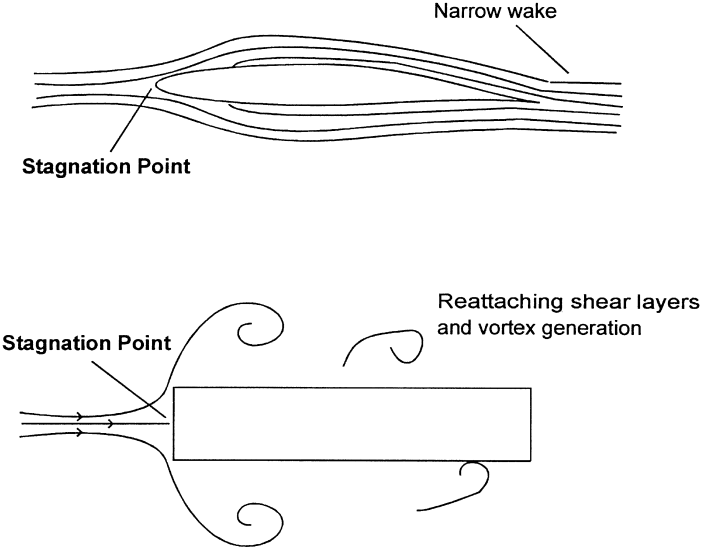

Figure 4.1 Flow around streamlined and bluff bodies.

to a surface. These layers are unstable in a sheet form and will roll up towards the wake, to form concentrated vortices, which are subsequently shed downwind.

In the case of the bluff body with a long 'after-body' in Figure 4.1, the separated shear layer 're-attaches' on to the surface. However, the shear layer is not fully stabilized and vortices may be formed on the surface, and subsequently roll along the surface.

4.2 Pressure and force coefficients

4.2.1 Bernoulli's equation

The region outside the boundary layers in the case of the airfoil, and the outer region of the bluff-body flow, are regions of *inviscid* (zero viscosity) and *irrotational* (zero vorticity) flow, and the pressure, p, and velocity, U, in the fluid are related by *Bernoulli's equation*

$$p + \frac{1}{2}\rho_a U^2 = \text{a constant} \tag{4.1}$$

Denoting the pressure and velocity in the region outside the influence of the body by p_0 and U_0, we have:

$$p + \frac{1}{2}\rho_a U^2 = p_0 + \frac{1}{2}\rho_a U_0^2$$

Hence,

$$p - p_0 = \frac{1}{2}\rho_a (U_0^2 - U^2)$$

The surface pressure on the body is usually expressed in the form a non-dimensional *pressure coefficient*:

$$C_p = \frac{p - p_0}{\frac{1}{2}\rho_a U_0^2} \tag{4.2}$$

In the region in which Bernoulli's equation holds:

$$C_p = \frac{\frac{1}{2}\rho_a (U_0^2 - U^2)}{\frac{1}{2}\rho_a U_0^2} = 1 - \left(\frac{U}{U_0}\right)^2 \tag{4.3}$$

At the stagnation point, where U is zero, equation (4.3) gives a pressure coefficient of one. This is the value measured by a *total* pressure or *pitot* tube pointing into a flow. The pressure $(1/2)\rho_a U_0^2$, is known as the *dynamic* pressure. Values of pressure coefficient near 1.0 also occur on the stagnation point on a circular cylinder, but the largest (mean) pressure coefficients on the windward faces of buildings are usually less than this theoretical value.

In the regions where the flow velocity is greater than u_0, the pressure coefficients are

negative. Strictly, Bernoulli's equation is not valid in the separated flow and wake regions, but reasonably good predictions of surface pressure coefficients can be obtained from equation (4.3), by taking the velocity, U, as that just outside the shear layers and wake region.

4.2.2 Force coefficients

Force coefficients are defined in a similar non-dimensional way to pressure coefficients:

$$C_F = \frac{F}{\frac{1}{2}\rho_a U_0^2 A} \tag{4.4}$$

where F is the total aerodynamic force, and A is a reference area (not necessarily the area over which the force acts). Often A is a projected frontal area.

In the case of long, or two-dimensional, bodies a force coefficient per unit length is usually used:

$$C_f = \frac{f}{\frac{1}{2}\rho_a U_0^2 b} \tag{4.5}$$

where f is the aerodynamic force per unit length, and b is a reference length, usually the breadth of the structure normal to the wind.

Aerodynamic forces are conventionally resolved into two orthogonal directions. These may be parallel and perpendicular to the wind direction (or mean wind direction in the case of turbulent flow), in which case the axes are referred to as *wind axes*, or parallel and perpendicular to a direction related to the geometry of the body (*body axes*). These axes are shown in Figure 4.2.

Following the terminology of aeronautics, the terms 'lift' and 'drag' are commonly used in wind engineering for cross-wind and along-wind force components, respectively. Substituting 'L' and 'D' for 'F' in equation (4.4) gives the definition of *lift and drag coefficients*.

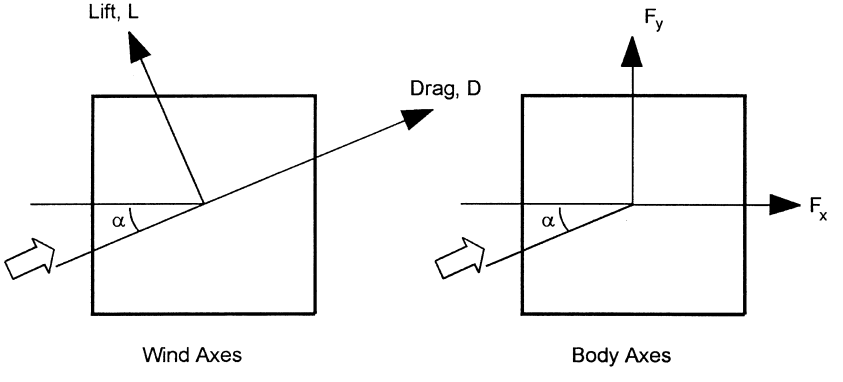

Figure 4.2 Wind axes and body axes.

The relationship between the forces and force coefficients resolved with respect to the two axes can be derived using trigonometry, in terms of the angle, α, between the sets of axes, as shown in Figure 4.3. α is called the *angle of attack* (or sometimes angle of incidence).

4.2.3 Dependence of pressure and force coefficients

Pressure and force coefficients are non-dimensional quantities, which are dependent on a number of variables related to the geometry of the body, and to the upwind flow characteristics. These variables can be grouped together into non-dimensional groups, using processes of dimensional analysis, or by inspection.

Assuming that we have a number of bluff bodies of geometrically similar shape, which can be characterized by a single length dimension (for example, buildings with the same ratio of height, width and length, and with the same roof pitch, characterized by their height, h), then the pressure coefficients for pressures at corresponding points on the surface of the body, may be a function of a number of other non-dimensional groups: π_1, π_2, π_3 etc……..

Thus,

$$C_p = f(\pi_1, \pi_2, \pi_3 \text{ etc...}) \tag{4.6}$$

Examples of relevant non-dimensional groups are:

h/z_0 (Jensen number)

where

- z_0 is the roughness length as discussed in Section 3.2.1;
- I_u, I_v, I_w are the turbulence intensities in the approaching flow;
- (ℓ_u/h), (ℓ_v/h), (ℓ_w/h) represent the ratios of turbulence length scales in the approaching flow, to the characteristic body dimension; and
- (Uh/ν) is the Reynolds number, where ν is the kinematic viscosity of air.

Equation (4.6) is relevant to the practice of wind-tunnel model testing, in which geometrically scaled models are used to obtain pressure (or force) coefficients for application

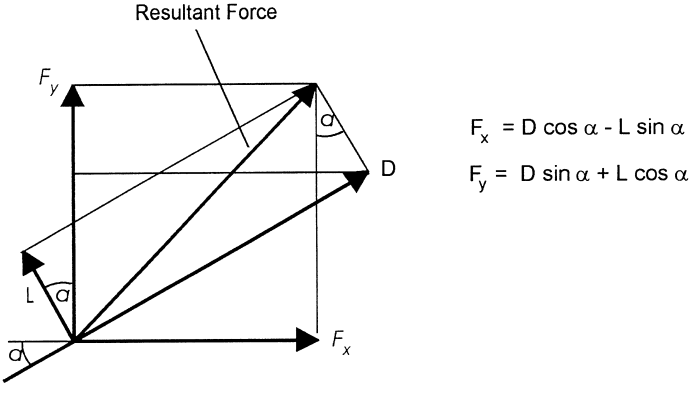

Figure 4.3 Relationships between resolved forces.

to full-scale prototype structures (see Section 7.4). The aim should be to ensure that all relevant non-dimensional numbers (π_1, π_2, π_3, etc.) should be equal in both model and full scale. This is difficult to achieve for all the relevant numbers, and methods have been devised for minimizing the errors resulting from this. Wind-tunnel testing techniques are discussed in Chapter 7.

4.2.4 Reynolds number

Reynolds number is the ratio of fluid inertia forces in the flow to viscous forces, and is an important parameter in all branches of fluid mechanics. In bluff-body flows, viscous forces, are only important in the surface boundary layers and free shear layers (Section 4.1) . The dependence of pressure coefficients on Reynolds number is often overlooked for sharp-edged bluff bodies, such as most buildings and industrial structures. For these bodies separation of flow occurs at sharp edges and corners, such as wall-roof junctions, over a very wide range of Reynolds number. However for bodies with curved surfaces, such as circular cylinders or arched roofs, the separation points *are* dependent on Reynolds number, and this parameter should be considered. However, the addition of turbulence to the flow reduces the Reynolds number-dependence for bodies with curved surfaces.

4.3 Flat plates and walls

4.3.1 Flat plates and walls normal to the flow

The flat plate, with its plane normal to the air stream, represents a common situation for wind loads on structures. Examples are: elevated hoardings and signboards, which are normally mounted so that their plane is vertical. Solar panels are another example but, in this case, the plane is inclined to the vertical to maximize the collection of solar radiation. Free-standing walls are another example, but the fact that they are attached to the ground, has a considerable effect on the flow and the resulting wind loading. In this section, some fundamental aspects of flow and drag forces on flat plates and walls are discussed.

For a flat plate or wall with its plane normal to the flow, the only aerodynamic force will be one parallel to the flow, i.e. a drag force. Then if p_W and p_L are the average pressures on the front (windward) and rear (leeward) faces respectively, the drag force, D, will be given by:

$$D = (p_W - p_L)\, A$$

where A is the frontal area of the plate or wall.

Then dividing both sides by $(1/2)\rho_a U^2 A$, we have:

$$C_D = C_{p,W} - C_{p,L} = C_{p,W} + (-C_{p,L}) \tag{4.7}$$

In practice, the windward wall pressure, p_W and pressure coefficient, $C_{p,W}$, varies considerably with position on the front face. The leeward (or 'base') pressure however, is nearly uniform over the whole rear face, as this region is totally exposed to the wake region, with relatively slow-moving air.

The mean drag coefficients for various plate and wall configurations are shown in Figure 4.4. The drag coefficient for a square plate in a smooth, uniform approach flow is about 1.1, slightly greater than the total pressure in the approach flow, averaged over the face

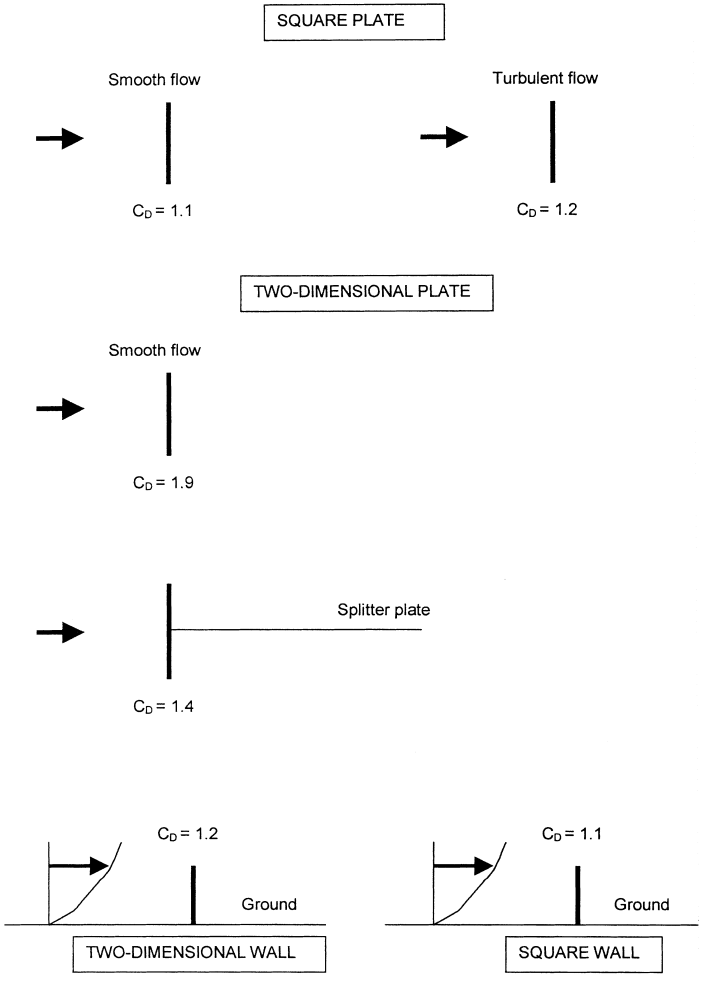

Figure 4.4 Drag coefficients for normal plates and walls.

of the plate. Approximately 60% of the drag is contributed by positive pressures (above static pressure) on the front face, and 40% by negative pressures (below static pressure) on the rear face (E.S.D.U., 1970).

The effect of free-stream turbulence is to increase the drag on the normal plate slightly. The increase in drag is caused by a decrease in leeward, or base pressure, rather than an increase in front face pressure. The hypothesis is that the free-stream turbulence causes an increase in the rate of entrainment of air into the separated shear layers. This leads to a reduced radius of curvature of the shear layers, and to a reduced base pressure, (Bearman, 1971).

Figure 4.4 also shows the drag coefficient on a long flat plate with a theoretically infinite width into the paper – the 'two-dimensional' flat plate. The drag coefficient of 1.9 is higher than that for the square plate. The reason for the increase on the wide plates can be explained as follows. For a square plate, the flow is deflected around the plate equally

around the four sides. The extended width provides a high-resistance flow path into (or out of) the paper, thus forcing the flow to travel faster over the top edge, and under the bottom edge. This faster flow results in more entrainment from the wake into the shear layers, thus generating lower base, or leeward face, pressure and higher drag.

Rectangular plates with intermediate values of width to height have intermediate values of drag coefficient. A formula given by E.S.D.U. (1970) for the drag coefficient on plates of height/breadth ratio in the range $1/30 < h/b < 30$, in smooth uniform flow normal to the plate, is reproduced in equation (4.8).

$$C_D = 1.10 + 0.02[(h/b) + (b/h)] \tag{4.8}$$

In the case of the two-dimensional plate, strong vortices are shed into the wake alternately from top and bottom, in a similar way to the bluff-body flow shown in Figure 4.1. These contribute greatly to the increased entrainment into the wake of the two-dimensional plate. Suppression of these vortices by a splitter plate, has the effect of reducing the drag coefficient to a lower value, as shown in Figure 4.4.

This suppression of vortex-shedding is nearly complete when a flat plate is attached to a ground plane, and becomes a wall, as shown in the lower sketch in Figure 4.4. In this case the approach flow will be of a boundary layer form with a wind speed increasing with height as shown. The value of drag coefficient, with U taken as the mean wind speed at the top of the wall, $\bar{U}_h$, is very similar for the two-dimensional wall, and finite wall of square planform, i.e. a drag coefficient of about 1.2 for an infinitely long wall. The effect of finite length of wall is shown in Figure 4.5. Little change in the mean drag coefficient occurs, although a slightly lower value occurs for an aspect ratio (length/height) of about 5 (Letchford and Holmes, 1994).

The case of two thin normal plates in series, normal to the flow, as shown in Figure 4.6, is an interesting one. At zero spacing, the two plates act like a single plate with a combined drag coefficient (based on the frontal area of one plate) of about 1.1, for a square plate. For spacings in the range of 0 to about 2 b, the combined drag coefficient is actually *lower* than that for a single plate, reaching a value of about 0.8 at a spacing of about 1.5 b, for two square plates. As the spacing is allowed to increase the combined drag coefficient then increases, so that, for very high spacings, the plates act like individual

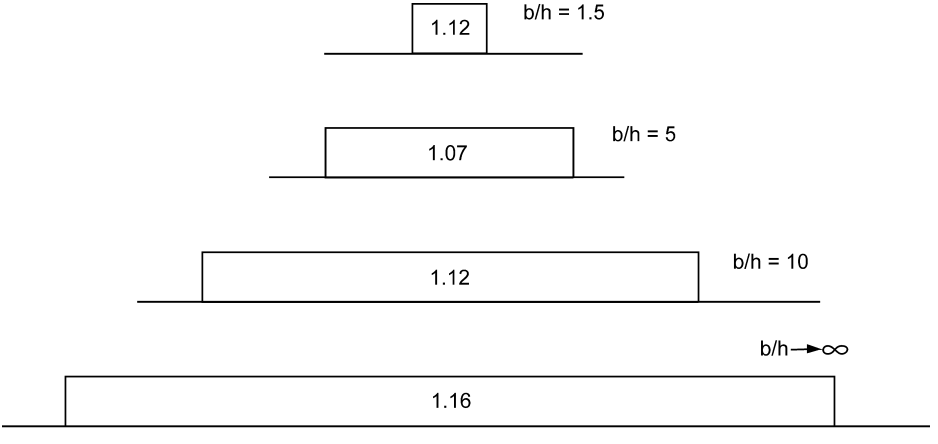

Figure 4.5 Mean drag coefficients on walls in boundary-layer flow.

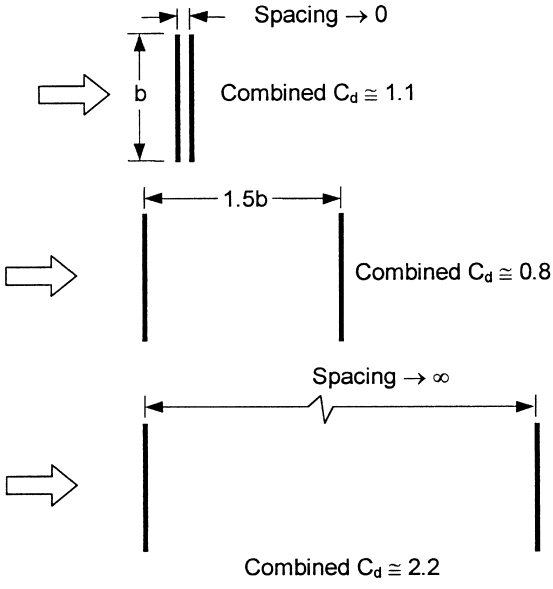

Figure 4.6 Drag coefficients for two square plates in series.

plates with no interference with each other, and a combined drag coefficient of about 2.2. The mechanism that produces the reduced drag at the critical spacing of 1.5 b has not been studied in detail, but clearly there is a large interference in the wake and in the vortex shedding, generated by the downstream plate.

The drag forces on two flat plates separated by small distances normal to the flow is also a relevant situation in wind engineering, with applications for clusters of lights or antennas together on a frame, for example. Experiments by Marchman and Werme (1982) found increases in drag of up to 15% when square, rectangular or circular plates were within half a width (or diameter) from each other.

If uniform porosity is introduced, the drag on a normal flat plate or wall, reduces as some air is allowed to flow through the plate, and reduce the pressure difference between front and rear faces. The reduction in drag coefficient can be represented by the introduction of a porosity factor, K_p, which is dependent on the solidity of the plate, δ, being the ratio of the 'solid' area of the plate, to the total elevation area, as indicated in equation (4.9).

$$C_{D,\delta} = C_D.K_p \tag{4.9}$$

K_p is not linearly related to the solidity. An approximate expression for K_p, which fits the data quite well for plates and walls with ratios of height to breadth between about 0.2 to 5, is given by equation (4.10).

$$K_p \cong 1 - (1 - \delta)^2 \tag{4.10}$$

Equation (4.10) has the required properties of equalling one for a value of δ equal to 1, i.e. an impermeable plate or wall, and tending to zero as the solidity tends to zero. For very small values of 2δ (for example an open truss plate made up of individual members), K_p tends to a value of 2δ, since, from equation (4.10),

$$K_p = 1 - (1 - 2\delta + \delta^2) \cong 2\delta,$$

since δ^2 is very small in comparison with 2δ for small δ.

Considering the application of this to the drag coefficient for an open-truss plate of square planform, we have from equations (4.9) and (4.10),

$$C_{D,At} \cong 1.1\ (2\delta)\ = 2.2\ \delta$$

where $C_{D,At}$ denotes that the drag coefficient, defined as in equation (4.4), is with respect to the total (enclosed) elevation area of A_t. With respect to the elevation area of the actual members in the truss A_m, the drag coefficient is larger, being given by:

$$C_{D,Am} = C_{D,At}\ (A_t/A_m)\ = C_{D,At}.(1/\delta) \cong 2.2$$

In this case of a very open plate, the members will act like isolated bluff bodies with individual values of drag coefficient of 2.2.

Cook (1990) discusses in detail the effect of porosity on aerodynamic forces on bluff bodies.

4.3.2 Flat plates and walls inclined to the flow

Figure 4.7 shows the case with the wind at an oblique angle of attack, α, to a two-dimensional flat plate. In this case the resultant force remains primarily at right angles to the plate surface, i.e. it is no longer a drag force in the direction of the wind. There is also a tangential component, or 'skin friction' force. However, this is not significant in comparison with the normal force, for angles of attack greater than about 10 degrees.

For small angles of attack, α, (less than 10 degrees), the normal force coefficient, C_N, with respect to the total plan area of the plate viewed normal to its surface, is given approximately by:

$$C_N \cong 2\pi\ \alpha, \tag{4.11}$$

where α is measured in radians, not in degrees.

Equation (4.11) comes from theory used in aeronautics. The 'centre of pressure', denoting the position of the line of action of the resultant normal force, is at, or near, one quarter of the height h, from the leading edge, again a result from aeronautical theory.

As the angle of attack, α, increases, the normal force coefficient, C_N, progressively increases towards the normal plate case ($\alpha = 90^o$), discussed in Section 4.3.1, with the centre of pressure at a height of 0.5 h. For example, the normal force coefficient for an angle of attack of 45 degrees, is about 1.5, with the centre of pressure at a distance of

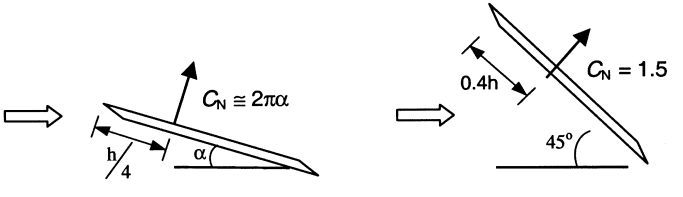

Figure 4.7 Normal force coefficients for an inclined two-dimensional plate.

about 0.4 h from the leading edge, as shown in Figure 4.7. The corresponding values for α equal to 30 degrees are about 1.2, and 0.38 h, (E.S.D.U., 1970).

Now, we will consider finite length walls and hoardings, at or near ground level, and hence in a highly sheared and turbulent boundary-layer flow. The mean net pressure coefficients at the windward end of the wall, for an oblique wind blowing at 45 degrees to the normal, are quite high due to the presence of a strong vortex system behind the wall. Some values of area-averaged mean pressure coefficients are shown in Figure 4.8; these high values are usually the critical cases for the design of free-standing walls and hoardings for wind loads.

4.4 Rectangular prismatic shapes

4.4.1 Drag on two-dimensional rectangular prismatic shapes

Understanding of the wind forces on rectangular prismatic shapes is clearly of importance for many structures, especially buildings of all heights and bridge decks. We will consider first the drag coefficients for two-dimensional rectangular prisms.

Figure 4.9 shows how the drag coefficient varies for two-dimensional rectangular prisms with sharp corners, as a function of the ratio, *d/b*, where *d* is the along-wind or afterbody length, and *b* is the cross-wind dimension. The flow is normal to a face of width *b*, and is 'smooth', i.e. the turbulence level is low. As previously shown in Figure 4.4, the value of the drag coefficient is 1.9 for (*d/b*) close to zero, i.e. for a flat plate normal to a flow stream. As (*d/b*) increases to 0.65 to 0.70, the drag coefficient increases to about 2.9 (e.g. Bearman and Trueman, 1972). The drag coefficient then decreases with increasing (*d/b*), reaching 2.0 for a square cross-section. The drag coefficient continues to decrease with further increases in (*d/b*), reaching about 1.0 for values of (*d/b*) of 5 or greater.

These variations can be explained by the behaviour of the free shear layers separating from the upstream corners. These shear layers are unstable, as was shown in Figure 4.1, and eventually form discrete vortices. During the formation of these vortices, air is entrained from the wake region behind the prism; it is this continual entrainment process which sustains a base pressure lower than the static pressure. As (*d/b*) increases to the range 0.65 to 0.70, the size of the wake decreases simply because of the increased volume of the prism occupying part of the wake volume. Thus the same entrainment process acts

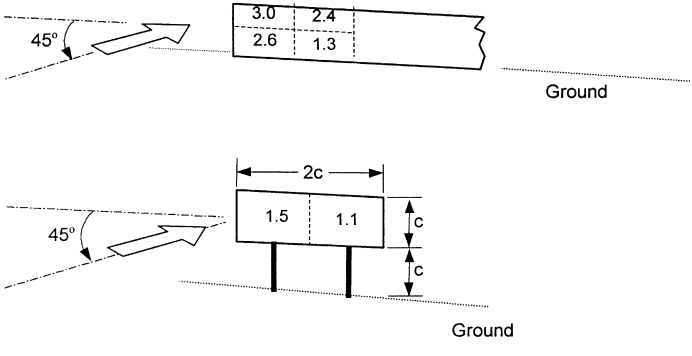

Figure 4.8 Area-averaged mean pressure coefficients on walls and hoardings for oblique wind directions.

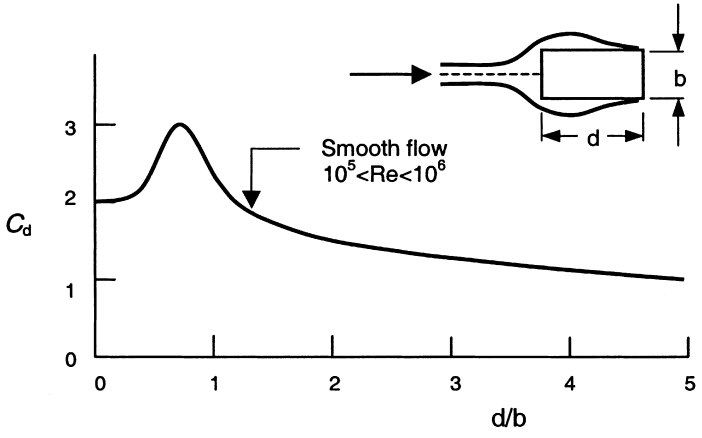

Figure 4.9 Drag coefficients for two-dimensional rectangular prisms in smooth flow.

on a smaller volume of wake air, causing the base pressure to decrease further, and the drag to increase. However, as (*d/b*) increases beyond 0.7, the rear, or downstream, corners interfere with the shear layers, and if the length *d* is long enough, the shear layers will stabilize, or 're-attach', on to the sides of the prisms. Although the attached shear layers will eventually separate again from the *rear* corners of the prism, the wake is smaller for prisms with long afterbodies (high *d/b*), and the entrainment is weaker. The result is a lower drag coefficient, as shown in Figure 4.9.

4.4.2 Effect of aspect ratio

The effect of a finite aspect ratio (height/breadth) is to introduce an additional flow path around the end of the body, and a means of increasing the pressure in the wake cavity. The reduced airflow normal to the axis results in a lower drag coefficient for finite length bodies in comparison to two-dimensional bodies of infinite aspect ratio. Figure 4.10 shows the drag coefficient for a square cross-section with one free end exposed to the flow, which was smooth (Scruton and Rogers, 1972). The aspect ratio in this case is calculated as 2*h*/*b*, where *h* is the height, since it is assumed that the flow is equivalent to that around a body with a 'mirror image' added to give an overall height of 2 h with two free ends.

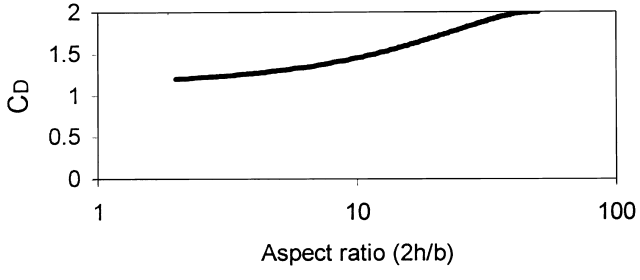

Figure 4.10 Effect of aspect ratio on drag coefficient for a square cross section.

4.4.3 *Effect of turbulence*

Free-stream turbulence containing scales of the prism dimensions or smaller can have significant effects on the mean drag coefficients of rectangular prisms, as well as producing fluctuating forces. As shown in Figure 4.4, the effect of free-stream turbulence on a flat plate normal to an air stream, is to increase the drag coefficient slightly (Bearman, 1971). This results from increased mixing and entrainment into the free shear layers induced by the turbulence. Observations have also shown a reduction in the radius of curvature of the mean shear layer position (Figure 4.11). As the after-body length increases, the drag first increases and then decreases, as occurs in smooth flow. However, because of the decrease in the mean radius of curvature of the shear layers caused by the free-stream turbulence, the (*d/b* ratio for maximum drag will decrease with increasing turbulence intensity, as shown in Figure 4.12) (Gartshore, 1973; Laneville *et al.,* 1975).

The drag coefficients for two-dimensional rectangular prisms on the ground in turbulent boundary-layer flow are shown in Figure 4.13. In comparison with rectangular prisms in smooth uniform flow (Figure 4.9), the drag coefficients, based on the mean wind speed at the height of the top of the prism, are much lower; because of the high turbulence in the boundary-layer flow, they do not show any maximum value.

Melbourne (1995) has discussed the important effects of turbulence on flow around bluff bodies in more detail.

4.4.4 *Drag and pressures on a cube and a prism*

The mean pressure distributions on a cube in a turbulent boundary layer flow are shown in Figure 4.14 (Baines, 1963). These pressure coefficients are based on the mean wind speed at the height of the top of the cube. The drag coefficient of 0.8 is lower than that of the two-dimensional square section prism (*d/h* equal to 1.0 in Figure 4.13). This is due

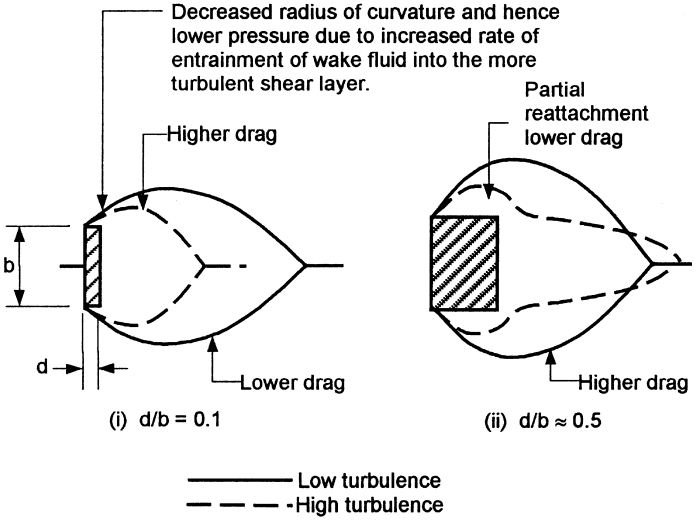

Figure 4.11 Effect of turbulence on shear layers from rectangular prisms (Laneville *et al.*, 1975).

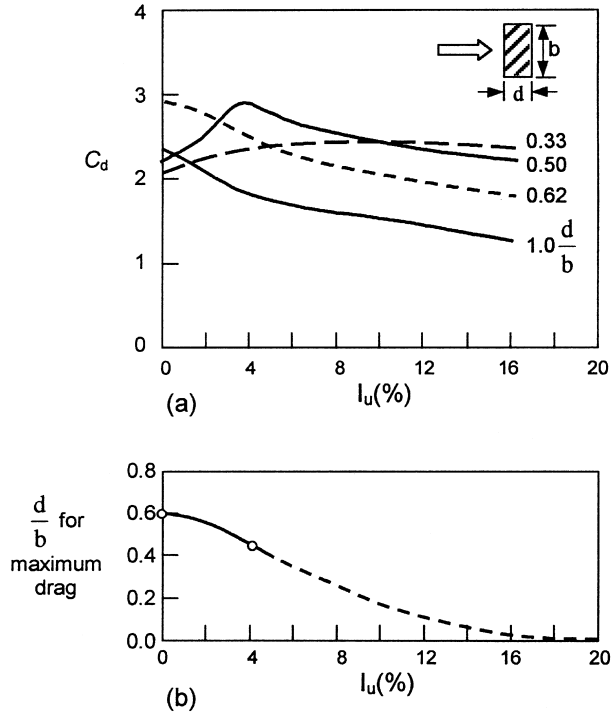

Figure 4.12 Effect of turbulence on drag coefficients for rectangular prisms (Laneville *et al.*, 1975).

to the three-dimensional flows that occur around the side walls of the block which increase the base pressure (decrease the negative pressure).

The mean pressure distribution on a tall prism of square cross-section in a turbulent boundary layer flow is shown in Figure 4.15, (Baines, 1963). This is representative of the pressure distribution on a tall building in the atmospheric boundary layer. The mean pressure coefficients are again based on the dynamic pressure calculated from the mean wind speed at the top of the prism. The effect of the vertical velocity profile on the windward wall pressure is clearly seen. The maximum pressure occurs at about 85% of the height. On the windward face of unshielded tall buildings, the strong pressure gradient can cause a strong downwards flow often causing high wind speeds which may cause problems for pedestrians at ground level.

4.4.5 Jensen number

For bluff bodies such as buildings, immersed in a turbulent boundary-layer flow, the ratio of characteristic body dimension, usually the height, h, in the case of a building, to the characteristic boundary-layer length, represented by the roughness length, z_o, is known as the Jensen number. In a classic series of experiments, Jensen (1958) established the need for equality of (h/z_o) in order for wind-tunnel mean pressure measurements on a model of a small building to match those in full scale. The effect is greatest on the roof and side

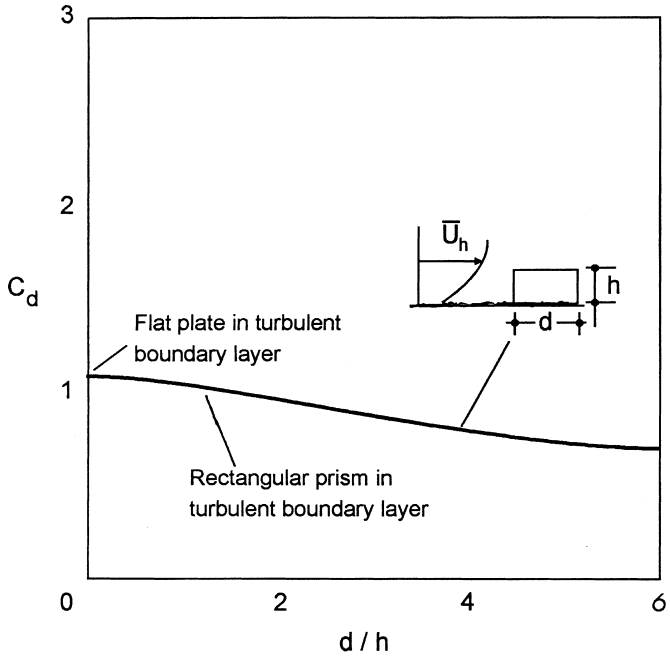

Figure 4.13 Mean drag coefficients for rectangular prisms in turbulent boundary-layer flow.

walls, where the increased turbulence in the flow over the rougher ground surfaces promotes shorter flow reattachment lengths.

For a given height, h, greater values of roughness length, z_o, and lower values of Jensen number, implies rougher ground surface and hence greater turbulence intensities at the height of the body. Thus fluctuating pressure coefficients also depend on Jensen number – decreasing Jensen number generally giving increasing root-mean-square pressure coefficients.

4.5 Circular cylinders

4.5.1 Effects of Reynolds number and surface roughness

For bluff bodies with curved surfaces such as the circular cylinder, the positions of the separation of the local surface boundary layers, are much more dependent on viscous forces than is the case with sharp-edged bodies. This results in a variation of drag forces with Reynolds number, which is the ratio of inertial forces to viscous forces in the flow (see Section 4.2.4). Figure 4.16 shows the variation of drag coefficient with Reynolds number for square section bodies with various corner radii (Scruton, 1981). The appearance of a 'critical' Reynolds number, at which there is a sharp fall in drag coefficient, occurs at a relatively low corner radius.

The various flow regimes for a circular cylinder with a smooth surface finish in smooth (low turbulence) flow are shown in Figure 4.17. The sharp fall in drag coefficient at a Reynolds number of about 2×10^5 is caused by a transition to turbulence in the surface boundary layers ahead of the separation points. This causes separation to be delayed to

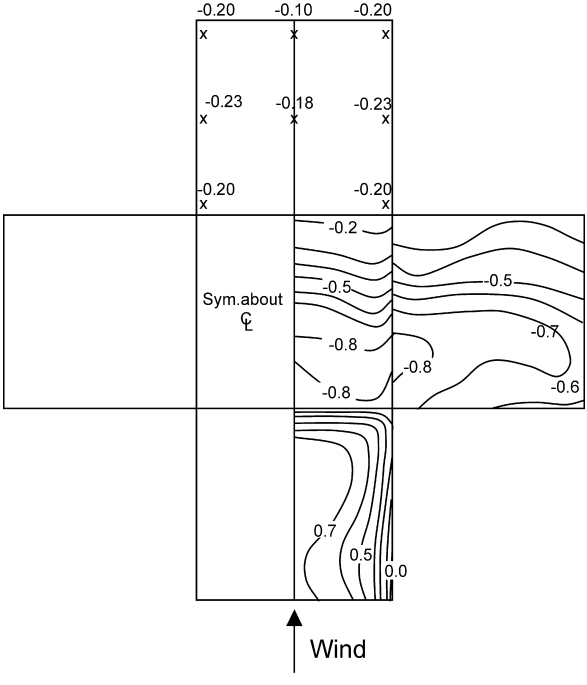

Figure 4.14 Mean pressure coefficients on a cube in turbulent boundary-layer flow (Baines, 1963).

an angular position of about 140 degrees from the front stagnation point, instead of 90 degrees, which is the case for subcritical Reynolds numbers. This delay in the separation results in a narrowing in the wake, and an increased (less negative) base pressure, and a lower drag coefficient. The pressure distributions at sub-critical and super-critical Reynolds numbers are shown in Figure 4.18.

As shown in Figure 4.16, the presence of a rough surface on a circular cylinder causes the critical Reynolds number range to be lower than that for a smooth cylinder. The minimum drag coefficient is higher for the rougher surfaces (E.S.D.U., 1980).

4.5.2 Effect of aspect ratio

The reduction in drag coefficient for a circular cylinder of finite aspect ratio (single free end) in smooth flow (subcritical) is shown in Figure 4.19 (Scruton and Rogers, 1972). This figure is analogous to Figure 4.10 for a square cross-section. As for the square section, the reduction in drag for a circular cylinder, results from the additional flow path provided by the free end on the body.

The mean pressure distribution around a circular cylinder with a height to diameter (aspect) ratio of 1, with its axis vertical in a turbulent boundary-layer flow is shown in Figure 4.20 (Macdonald *et al*., 1988). The minimum mean pressure coefficient on the side occurs at angular position of about 80 degrees, and is about –1.2, lower in magnitude than the value of about –2.0 for a two-dimensional cylinder in supercritical flow (see Figure 4.18). The minimum $\bar{C}_p$ increases in magnitude with increasing aspect ratio, reaching the two-dimensional value at an aspect ratio of about 2.0.

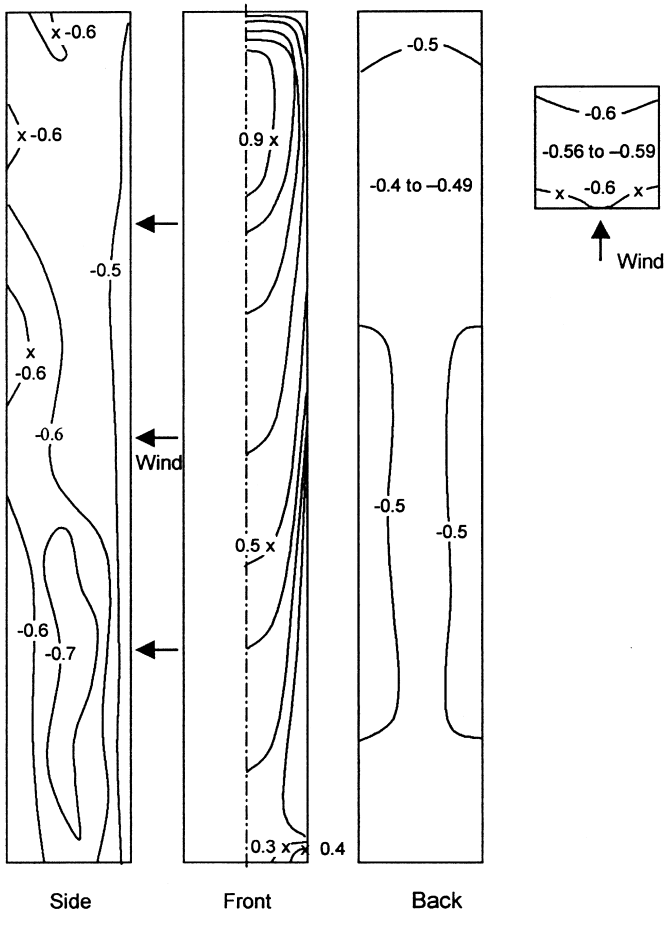

Figure 4.15 Mean pressure coefficients on a tall prism in turbulent boundary-layer flow (Baines, 1963).

4.6 Fluctuating forces and pressures

4.6.1 Introduction

The turbulent and fluctuating nature of wind flow in the atmospheric boundary layer has been described in Chapter 3. This and the unstable nature of flow around bluff bodies which results in flow separations, and sometimes re-attachments, produces pressures and forces on bodies in the natural wind which are also highly fluctuating.

The main sources of the fluctuating pressures and forces are as follows:

- Natural turbulence or gustiness in the free stream flow. This is often called 'buffeting'. If the body dimensions are small relative to the length scales of the turbulence, the pressure and force variations will tend to follow the variations in velocity (see Section 4.6.2 on the quasi-steady assumption)

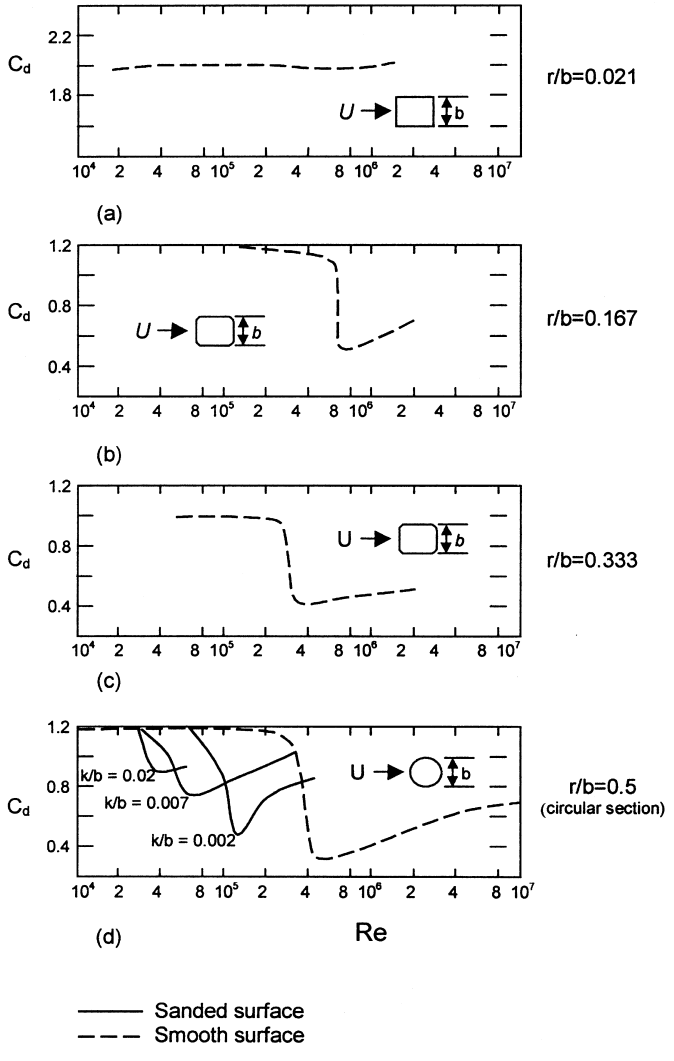

Figure 4.16 Effect of Reynolds number, corner radius and surface roughness on drag coefficients of square sections (Scruton, 1981).

- Unsteady flow generated by the body itself, by phenomena such as separations, reattachments and vortex shedding
- Fluctuating forces due to movement of the body itself (e.g. aerodynamic damping).

The third source arises only for very flexible vibration-prone 'aeroelastic structures'. In the following sections, only the first two sources will be considered.

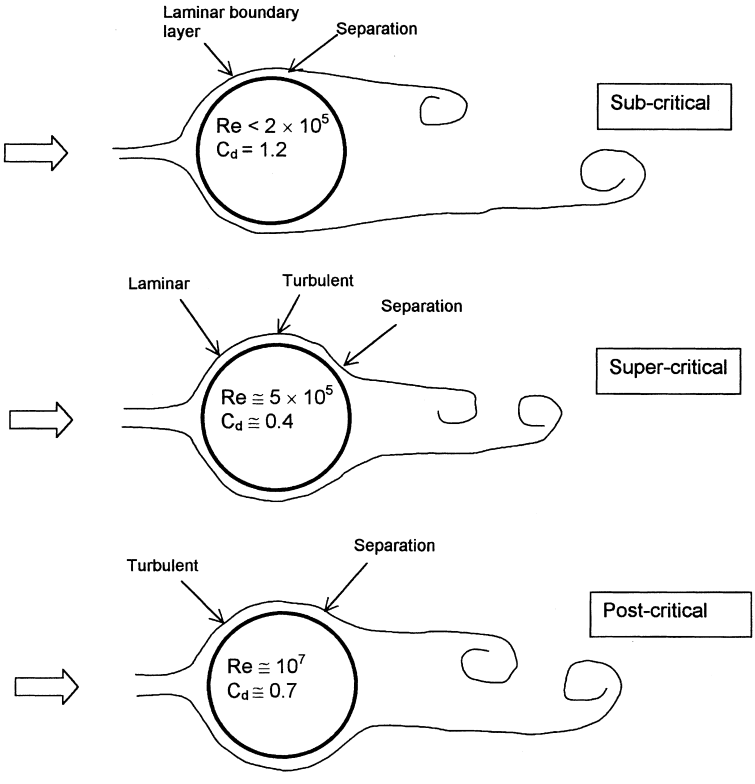

Figure 4.17 Flow regimes for a circular cylinder in smooth flow.

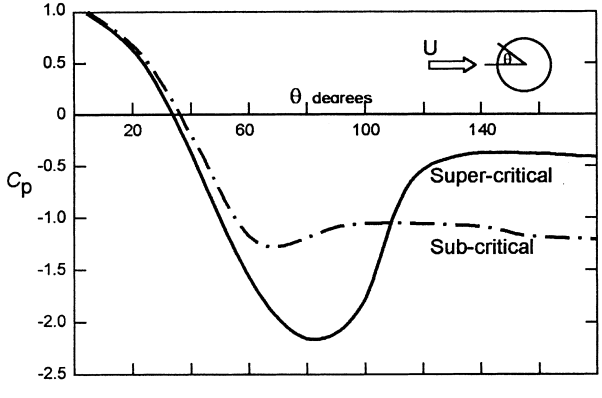

Figure 4.18 Pressure distributions around a two-dimensional circular cylinder at subcritical and super-critical Reynolds numbers.

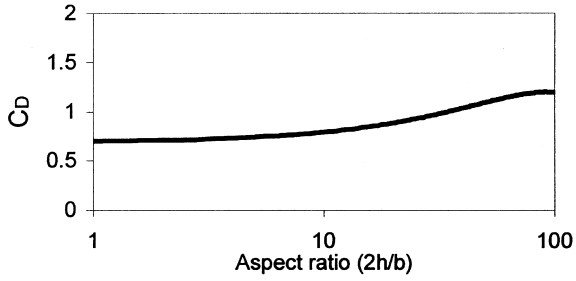

Figure 4.19 Effect of aspect ratio on drag coefficient of a circular cylinder (subcritical Reynolds number).

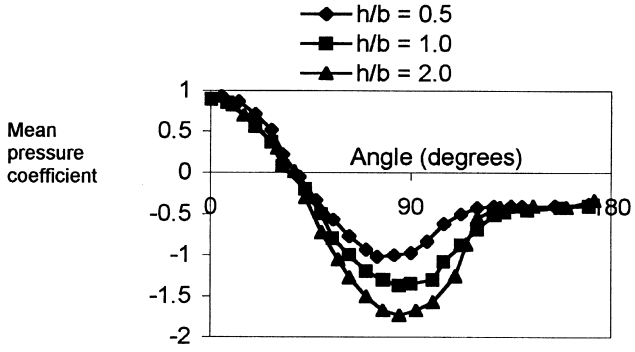

Figure 4.20 Effect of aspect ratio (height/diameter) on pressure distributions around circular cylinders.

4.6.2 The quasi-steady assumption

The 'quasi-steady' assumption is the basis of many wind loading codes and standards. The fluctuating pressure on a structure is assumed to follow the variations in longitudinal wind velocity upstream. Thus,

$$p(t) = C_{po}(1/2)\rho_a[U(t)]^2 \tag{4.12}$$

where C_{po} is a quasi-steady pressure coefficient.

Expanding $U(t)$ into its mean and fluctuating components,

$$p(t) = C_{po}(1/2)\rho_a[\bar{U} + u'(t)]^2 = C_{po}(1/2)\rho_a[\bar{U}^2 + 2\bar{U}\,u'(t) + u'(t)^2] \tag{4.13}$$

Taking mean values,

$$\bar{p} = C_{po}\,(1/2)\,\rho_a\,[\bar{U}^2 + \sigma_u{}^2]$$

For small turbulence intensities, $\sigma_u{}^2$ is small in comparison with $\bar{U}^2$. Then the quasi-steady pressure coefficient, C_{po}, is approximately equal to the mean pressure coefficient, $\bar{C}_p$.

Then,

$$\bar{p} \cong C_{po}(1/2)\rho_a \bar{U}^2 = \bar{C}_p(1/2)\rho_a \bar{U}^2 \tag{4.14}$$

Subtracting the mean values from both sides of (4.13), we have,

$$p'(t) \ = C_{po}\ (1/2)\ \rho_a\ [2\bar{U}\ u'(t)\ + u'(t)^2]$$

Neglecting the second term in the square brackets (valid for low turbulence intensities), squaring and taking mean values,

$$\overline{p'^2} \cong \bar{C}_p^2(1/4)\rho_a^2[4\bar{U}^2\overline{u'^2}] = \bar{C}_p^2\rho_a^2\bar{U}^2\overline{u'^2} \tag{4.15}$$

Equation (4.15) is a quasi-steady relationship between mean square pressure fluctuations and mean square longitudinal velocity fluctuations.

To predict peak pressures by the quasi-steady assumption,

$$\hat{p},\ \check{p} = C_{po}(1/2)\rho_a[\hat{U}^2] \cong \bar{C}_p(1/2)\rho_a[\hat{U}^2] \tag{4.16}$$

Thus according to the quasi-steady assumption, we can predict peak pressures (maxima and minima) by using mean pressure coefficients with a peak gust wind speed. This is the basis of many codes and standards that use a peak gust as a basic wind speed (see Chapter 15). Its main disadvantage is that building induced pressure fluctuations (the second source described in Section 4.6.1) are ignored. Also when applied to wind pressures over large areas, it is conservative, because full correlation of the pressure peaks is implied. These effects and the way they are treated in codes and standards are discussed in Chapter 15.

4.6.3 Body-induced pressure fluctuations and vortex shedding forces

The phenomena of separating shear layers and vortex shedding have already been introduced in Sections 4.1, 4.3.1, 4.4.1 and 4.5 in descriptions of the flow around some basic bluff-body shapes. These phenomena occur whether the flow upstream is turbulent or not, and the resulting surface pressure fluctuations on a bluff body, can be distinguished from those generated by the flow fluctuations in the approaching flow.

The regular vortex shedding into the wake of a long bluff body results from the rolling-up of the separating shear layers alternately one side, then the other, and occurs on bluff bodies of all cross-sections. A regular pattern of decaying vortices, known as the von Karman vortex 'street', appears in the wake. Turbulence in the approaching flow tends to make the shedding less regular, but the strengths of the vortices are maintained, or even enhanced. Vibration of the body may also enhance the vortex strength, and the vortex-shedding frequency may change to the frequency of vibration, in a phenomenon known as *lock-in*.

As each vortex is shed from a bluff body, a strong cross-wind force is induced towards the side of the shed vortex. In this way, the alternate shedding of vortices induces a nearly harmonic (sinusoidal) cross-wind force variation on the structure.

For a given cross-sectional shape, the frequency of vortex shedding, n_s, is proportional to the approaching flow speed, and inversely proportional to the width of the body. It may be expressed in a non-dimensional form, known as the *Strouhal number, St*.

$$St = \frac{n_s b}{\bar{U}} \tag{4.17}$$

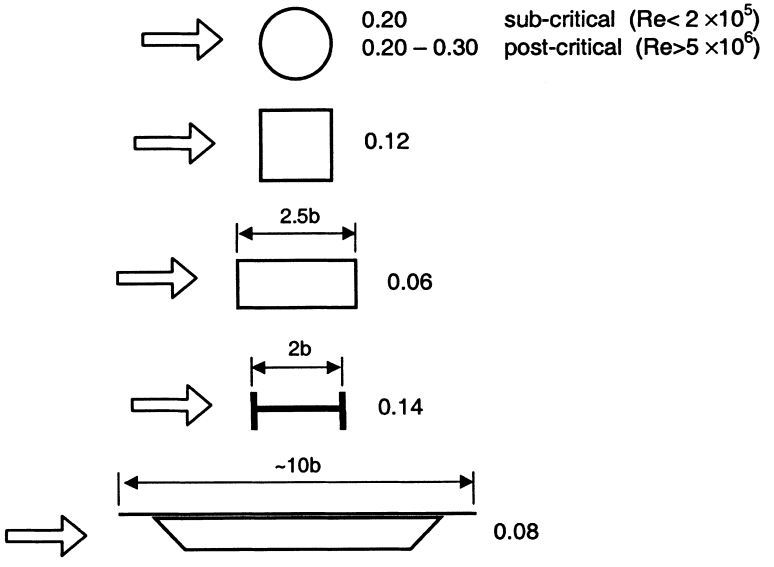

Figure 4.21 Strouhal numbers for vortex shedding for various cross sections.

where, b is the cross-wind body width and $\bar{U}$ is the mean flow speed.

The Strouhal number varies with the shape of the cross-section, and for circular and other cross-sections with curved surfaces varies with Reynolds number. Some representative values of Strouhal number for a variety of cross-sections, are shown in Figure 4.21.

The variation with Reynolds number for a circular cylinder is shown in Figure 4.22

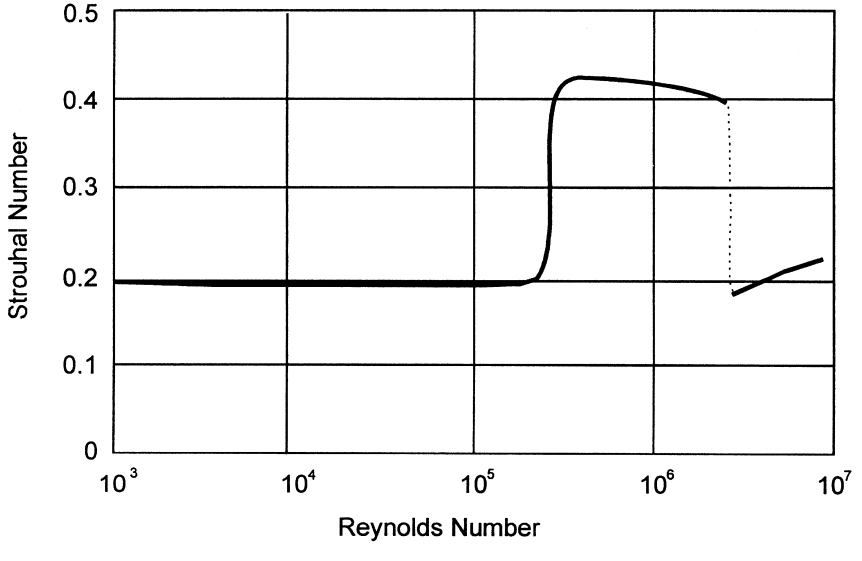

Figure 4.22 Strouhal numbers versus Reynolds number for circular cylinders.

(Scruton, 1963; Schewe, 1983). In the subcritical range, up to a Reynolds number of 2×10^5, the Strouhal number is quite constant at a value of 0.20. In the critical Reynolds number range, coinciding with the sharp fall in drag coefficient (see Figure 4.16), the Strouhal number jumps to 0.3 and then 0.48, although in this range the vortex shedding is random, and not clearly defined. A slightly decreasing Strouhal number to about 0.4, in the supercritical range, is followed by a fall to about 0.2 again, at a Reynolds number of 2×10^6. Helical strakes (Figure 4.23) are often used to inhibit vortex shedding and the resulting cross-wind forces on structures with circular sections such as chimney stacks (Scruton and Walshe, 1957).

4.6.4 Fluctuating pressure and force coefficients

The root-mean-square fluctuating (standard deviation) pressure coefficient at a point on a bluff body is defined by:

$$C'_p = \frac{\sqrt{\overline{p'^2}}}{\frac{1}{2}\rho_a \bar{U}^2} \tag{4.18}$$

$\sqrt{\overline{p'^2}}$ is the root-mean-square fluctuating, or standard deviation, pressure (also denoted by σ_p).

The root-mean-square fluctuating sectional force coefficient per unit length of a two-dimensional cylindrical or prismatic body is defined by:

$$C'_f = \frac{\sqrt{\overline{f'^2}}}{\frac{1}{2}\rho_a \bar{U}^2 b} \tag{4.19}$$

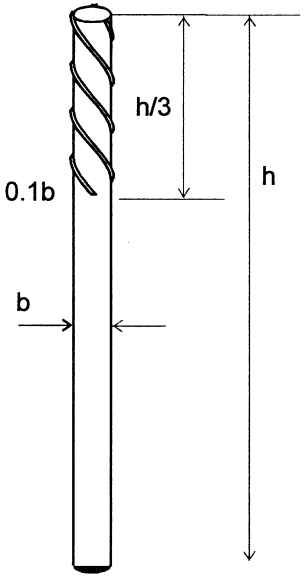

Figure 4.23 Helical strakes for inhibiting vortex shedding.

$\sqrt{\overline{f'^2}}$ is the root-mean-square fluctuating force per unit length. b is a reference dimension – usually the cross-wind breadth.

For a whole body,

$$C'_F = \frac{\sqrt{\overline{F'^2}}}{\frac{1}{2}\rho_a \bar{U}^2 A} \tag{4.20}$$

$\sqrt{\overline{F'^2}}$ is the root-mean-square fluctuating force acting on the complete body. A is a reference area – usually the frontal area.

The total fluctuating force acting on a cylindrical body of finite length, can be calculated from the fluctuating sectional force, knowing the correlation function, or correlation length.

With the quasi-steady assumption (Section 4.6.2), the root-mean-square fluctuating pressure coefficient can be estimated from equations (4.15) and (4.18):

$$C'_p = \frac{\sqrt{\overline{p'^2}}}{\frac{1}{2}\rho_a \bar{U}^2} \approx \frac{\bar{C}_p \rho_a \bar{U} \sqrt{\overline{u'^2}}}{\frac{1}{2}\rho_a \bar{U}^2} = 2\bar{C}_p I_u \tag{4.21}$$

where I_u is the longitudinal turbulence intensity $\left(= \frac{\sqrt{\overline{u'^2}}}{\bar{U}} \text{ or } \frac{\sigma_u}{\bar{U}} \right)$, as defined in Section 3.3.1.

Similarly the r.m.s. fluctuating drag coefficient can be estimated using the quasi-steady assumption:

$$C'_D \approx 2\bar{C}_D I_u \tag{4.22}$$

Fluctuating forces in the cross-wind direction are usually determined by experiment, however. Measurements have shown that square cross-sections experience stronger cross-wind fluctuating forces due to vortex shedding, than do circular cross-sections. Figure 4.24 shows the variation of r.m.s. fluctuating cross-wind force per unit length, for a circular cylinder, as a function of Reynolds number (Wootton and Scruton, 1970). The value is around 0.5 at subcritical Reynolds numbers, falling to much lower values in the critical and supercritical ranges, coinciding with a reduction in drag coefficient (Section 4.5.1).

The fluctuating cross-wind force coefficient for a square cross-section with sharp corners is higher than that for a circular section, due to the greater strength of the shed vortices. In smooth flow, the r.m.s. fluctuating cross-wind force coefficient is about 1.3; this drops to about 0.7 in turbulent flow of 10% intensity (Vickery, 1966).

4.6.5 Correlation length

The spatial correlation coefficient for fluctuating forces at two points along a cross-section is defined by:

$$\rho = \frac{\overline{f'_1(t) f'_2(t)}}{\overline{f'^2}} = \frac{\overline{f'_1(t) f'_2(t)}}{\sigma_f^2} \tag{4.23}$$

where $f'_1(t), f'_2(t)$ are the fluctuating forces per unit length at two sections along a cylindrical

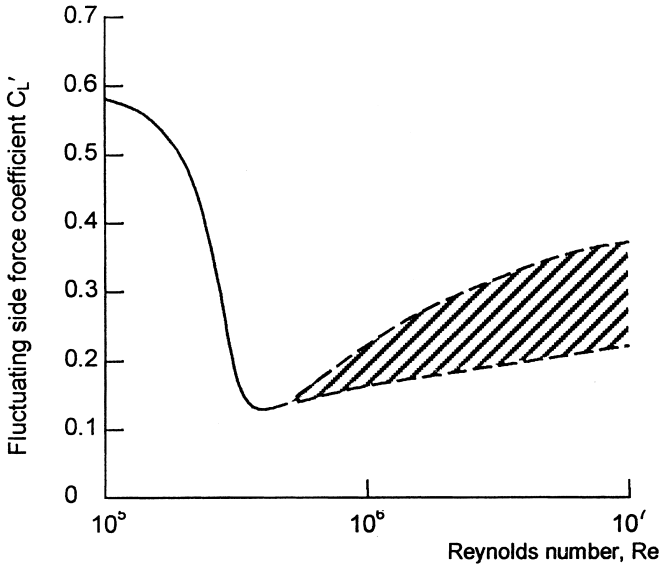

Figure 4.24 Variation of fluctuating cross-wind force coefficient per unit length with Reynolds number for a circular cylinder (Wootton and Scruton, 1970. Reproduced by permission of C.I.R.I.A., London.).

or prismatic body. (This was previously discussed in relation to atmospheric turbulence in Section 3.3.5.)

We have assumed that the mean square fluctuating force per unit length is constant along the body, so that:

$$\overline{f_1'^2} = \overline{f_2'} = \overline{f'^2}$$

As the separation distance, y, between the two sections 1 and 2 approaches zero, the correlation function, $\rho(y)$, approaches 1. As the separation distance becomes very large, $\rho(y)$ tends to zero; this means there is no statistical relationship between the fluctuating forces.

The *correlation length,* ℓ, is then defined as:

$$\ell = \int_0^\infty \rho(y)dy \tag{4.24}$$

The correlation length is thus the area under the graph of $\rho(y)$ plotted against y.

Measurements of correlation length for a smooth circular cylinder in smooth flow are shown in Figure 4.25 (Wootton and Scruton, 1970). The correlation length falls from about five diameters to one diameter over the critical Reynolds number range.

4.6.6 Total fluctuating forces on a slender body

Consider a long cylindrical, or prismatic, body of length, L, subjected to fluctuating wind forces along its length. Divide the body into a large number, N, of sections of width, δy_1,

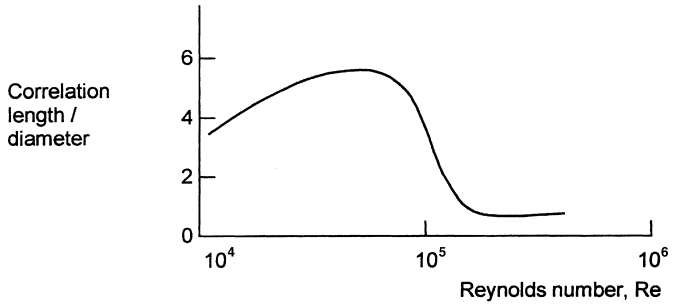

Figure 4.25 Variation of correlation length with Reynolds number for a stationary circular cylinder (Wootton and Scruton, 1970. Reproduced by permission of C.I.R.I.A., London.).

δy_2,..., δy_N, as shown in Figure 4.26. Assume that the mean square fluctuating force is the same at all sections.

At any section, *i*, the total force per unit length can be separated into a mean, or time-averaged, component, and a fluctuating component with a zero mean:

$$f_i(t) = \bar{f}_i + f_i'(t) \tag{4.25}$$

The total mean force acting on the whole body is given by:

$$\bar{F} = \Sigma\, \bar{f}_i\, \delta y_i$$

where the summation is taken from *i* equal to 1 to *N*.

As we let the number of sections tend to infinity, δy_i tends to zero, and the right-hand side becomes an integral:

$$\bar{F} = \int_0^L \bar{f}_i dy_i \tag{4.26}$$

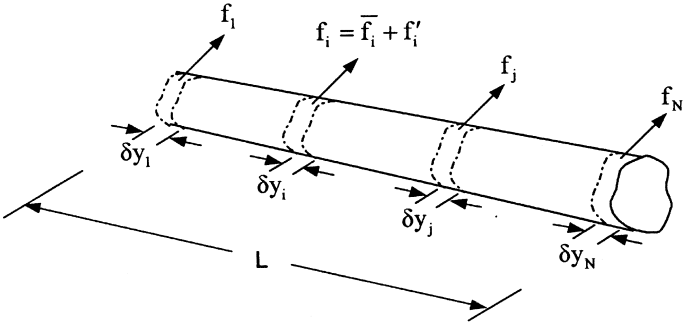

Figure 4.26 Sectional force fluctuations on a long slender body.

The instantaneous fluctuating force on the body as a whole is:

$$F'(t) = \Sigma f_i'(t)\,\delta y_i = f_1'(t)\,\delta y_1 + f_2'(t)\,\delta y_2 + \ldots f_N'(t)\,\delta y_N$$

Squaring both sides,

$$[F'(t)]^2 = [f_1'(t)\,\delta y_1 + f_2'(t)\,\delta y_2 + \ldots f_N'(t)\delta y_N]^2 = [f_1'(t)\delta y_1]^2 + [f_2'(t)\,\delta y_2]^2$$
$$.. + [f_N'(t)\,\delta y_N]^2 + f_1'(t)\,f_2'(t)\,\delta y_1\delta y_2 + f_1'(t)\,f_3'(t)\,\delta y_1\delta y_3 + \ldots = \sum_i^N \sum_j^N f_i'(t) f_j'(t)\delta y_i \delta y_j$$

Now taking means (time averages) of both sides,

$$\overline{F'^2} = \sum_i^N \sum_j^N \overline{f_i'(t) f_j'(t)}\delta y_i \delta y_j \tag{4.27}$$

As δy_i, δy_j tend to zero,

$$\overline{F'^2} = \int_0^L \int_0^L \overline{f_i'(t) f_j'(t)}\, dy_i dy_j \tag{4.28}$$

Equations (4.27) and (4.28) are important equations, which illustrate how to obtain a total fluctuating force from the fluctuating force on small elements. The integrand in equation (4.28) is the *covariance* of the sectional force fluctuations.

Now assume that the integrand can be written in the form:

$$\overline{f_i'(t) f_j'(t)} = \overline{f'^2}\rho(y_i - y_j)$$

where $\rho(y_i - y_j)$ is the correlation coefficient for the fluctuating sectional forces, which is assumed to be a function of the separation distance, $(y_i - y_j)$, but not of the individual positions y_i and y_j, i.e. we assume that the wind forces are horizontally, or vertically, *homogeneous*.

Then,

$$\overline{F'^2} = \overline{f'^2(t)} \int_0^L \int_0^L \rho(y_i - y_j)\, dy_i dy_j \tag{4.29}$$

This is the fundamental equation for the total mean square fluctuating force on the body, in terms of the mean square fluctuating force per unit length.

By introducing a new variable equal to $(y_i - y_j)$, equation (4.29) can be written:

$$\overline{F'^2} = \overline{f'^2} \int_0^L dy_j \int_{-y_j}^{L-y_j} \rho(y_i - y_j)\, d(y_i - y_j) \tag{4.30}$$

Equations (4.29) or (4.30) can be evaluated in two special cases:

4.6.6.1 (1) Full correlation

This assumption implies that $\rho(y_i - y_j)$ equals 1 for all separations, $(y_i - y_j)$. Then equation (4.29) becomes:

$$\overline{F'^2} = \overline{f'^2(t)}L^2$$

In this case the fluctuating forces are treated like static forces.

4.6.6.2 (2) Rapidly decreasing correlation length

In this case, ℓ is much less than L, and the second part of equation (4.29) can be approximated by:

$$\int_{-y_j}^{L-y_j} \rho(y_i - y_j)d(y_i - y_j) = \int_{-\infty}^{\infty} \rho(y_i - y_j)d(y_i - y_j) = 2\ell,$$

from equation (4.24).

Then from equation (4.30),

$$\overline{F'^2} = \overline{f'^2(t)}L.2\ell \tag{4.31}$$

Thus the mean square total fluctuating force is directly proportional to the correlation length, ℓ. This is an important result that is applicable to structures such as slender towers.

4.7 Summary

This chapter has attempted to summarize the relevant aspects of bluff-body aerodynamics, itself a large subject with applications in many fields, to wind loads on structures. The basic fluid mechanics of stagnation, separation and wakes has been described, and pressure and force coefficients are defined. The characteristics of pressures and forces on the basic shapes of flat plates and walls, cubes and rectangular prisms, and circular cylinders have been described. The effect of turbulence and the ground surface are covered.

Fluctuating pressures and forces, particularly those generated by upwind turbulence, and the regular shedding of vortices by a bluff body are discussed. The concept of correlation length and the averaging process by which fluctuating total forces on a body can be calculated are described.

References

Baines, W. D. (1963) 'Effects of velocity distributions on wind loads and flow patterns on buildings', *Proceedings, International Conference on Wind Effects on Buildings and Structures*, Teddington U.K., 26–28 June, 198–225.

Bearman, P. W. (1971) 'An investigation of the forces on flat plates normal to a turbulent flow', *Journal of Fluid Mechanics* 46: 177–98.

Bearman, P. W. and Trueman, D. H. (1972) 'An investigation of the flow around rectangular cylinders', *Aeronautical Quarterly* 23: 229–37.

Cook, N. J. (1990) *The Designer's Guide to Wind Loading of Building Structures. Part 2 Static Structures*. Building Research Establishment and Butterworths, London.

E.S.D.U. (1970) Fluid forces and moments on flat plates. Engineering Sciences Data Unit (E.S.D.U. International), E.S.D.U. Data Item 70015.

—— (1980) Mean forces, pressures and flow field velocities for circular cylindrical structures: single cylinder with two-dimensional flow. Engineering Sciences Data Unit (E.S.D.U. International, London, U.K.), E.S.D.U. Data Item 80025.

Gartshore, I. S. (1973) 'The effects of freestream turbulence on the drag of rectangular two-dimensional prisms', University of Western Ontario, Boundary Layer Wind Tunnel Report, BLWT–4–73.

Laneville, A., Gartshore, I. S. and Parkinson, G. V. (1975) 'An explanation of some effects of turbulence on bluff bodies', *Fourth International Conference on Wind Effects on Buildings and Structures,* London, U.K., September.

Letchford, C. W. and Holmes, J. D. (1994) 'Wind loads on free-standing walls in turbulent boundary layers', *Journal of Wind Engineering and Industrial Aerodynamics* 51: 1–27.

Jensen, M. (1958) 'The model law for phenomena in the natural wind', *Ingenioren* 2: 121–8.

Macdonald, P. A., Kwok, K. C. S., and Holmes J. D. (1988) 'Wind loads on circular storage bins, silos and tanks: I point pressure measurements on isolated structures', *Journal of Wind Engineering and Industrial Aerodynamics* 31: 165–88.

Marchman, J. F. and Werme, T. D. (1982) 'Mutual interference drag on signs and luminaires', *A.S.C.E. Journal of the Structural Division* 108: 2235–44.

Melbourne, W. H. (1995) 'Bluff body aerodynamics for wind engineering', in *A State of the Art in Wind Engineering*. Wiley Eastern Limited.

Schewe, G. (1983) 'On the force fluctuations acting on a circular cylinder in crossflow from subcritical up to transcritical Reynolds Numbers', *Journal of Fluid Mechanics* 133: 265–85.

Scruton, C. (1963) 'On the wind-excited oscillations of stacks, towers and masts', *Proceedings, International Conference on Wind Effects on Buildings and Structures*, Teddington, U.K. 26–28 June, 798–832.

—— (1981) *An Introduction to Wind Effects on Structures.* Oxford University Press.

Scruton, C. and Rogers, E. W. E. (1972) 'Steady and unsteady wind loading of buildings and structures', *Philosophical Transactions Royal Society, A* 269: 353–83.

Scruton, C. and Walshe, D. E. J. (1957) 'A means for avoiding wind-excited oscillations of structures of circular or near-circular cross section', National Physical Laboratory (U.K.), N.P.L. Aero Report 335 (unpublished).

Vickery, B. J. (1966) 'Fluctuating lift and drag on a long cylinder of square cross-section in a smooth and turbulent flow', *Journal of Fluid Mechanics* 25: 481–94.

Wootton, L. R. and Scruton, C. (1970) 'Aerodynamic stability', *Proceedings, CIRIA Seminar on the Modern Design of Wind-Sensitive Structures*, 18 June, London: C.I.R.I.A., 6 Storey's Gate, London, U.K., 65–81.